





Edge states of topological acoustic phonons in graphene zigzag nanoribbonsZhong-Ke Ding , Yu-Jia Zeng , Hui Pan , Nannan Luo, Jiang Zeng, Li-Ming Tang, and Ke-Qiu Chen ^{*}
Department of Applied Physics, School of Physics and Electronics, Hunan University, Changsha 410082, China

(Received 24 April 2022; revised 4 September 2022; accepted 7 September 2022; published 12 September 2022)

The tight-binding method is an effective way to study topological insulators. However, an intrinsic element, i.e., the acoustic sum rule (ASR) in phonon systems, has often been overlooked when constructing the Wannier tight-binding phonon Hamiltonian, which results in edge states of acoustic modes rarely observed in previous works. In the present work, we show that the topological acoustic edge states in graphene need to be assessed by ASR. Interestingly, when the inversion-time-reversal symmetry is broken, the distributions of some edge states will mutate from two edges of the nanoribbon to one edge. Moreover, some other topological phonon modes, which are different from previous reports, have also been observed. Our results would shed light on the method for searching topological phonon states, and provide effective strategies for designing phononic devices.

DOI: [10.1103/PhysRevB.106.L121401](https://doi.org/10.1103/PhysRevB.106.L121401)

Introduction. The last dozen years have witnessed the rapid development of topological phononics, which has been attracting tremendous interest in how to manipulate phonons more effectively [1–6]. In earlier studies, in addition to theoretical exploration [7–18], topological phonon states have also been realized in various macroscopic artificial lattices [19–21]. However, due to the importance of atomic lattice vibrations in material physics, more and more attention has been paid to natural crystalline materials. In recent years, various topological phonon states, such as Dirac phonons [22–24], Weyl point phonons [25–30], nodal-line phonons [29,31,32], nodal-ring phonons [33,34], and nodal-net phonons [35], have also been discovered in natural crystalline materials. The exploration of topological phononics in real materials may be of great importance in some potential applications, such as phononic devices [16,18,36,37], thermal metamaterial [38], topological transport [39,40], and thermoelectrics [41,42].

In the development of topological phononics, it is very important to introduce topological related concepts and methods into phononic systems legitimately. Like electrons, phonons, as a kind of elementary excitation, are also described by the Bloch wave function. Hence, it is possible to extend the topological concepts of electronic systems to phononic systems. However, given the fact that electrons and phonons are different in equations of motion, topological phononics should not be viewed as a simple extension of topological electronics [4,6]. Hence, new equations were proposed successively to describe the dynamical behavior of phonons [3,7,16] so that the topological concepts of phonons, such as Berry curvature, Chern number, and \mathbb{Z}_2 invariant, can be defined more rigorously. For example, based on eigenvalue equation of non-Hermitian phonon Hamiltonian, the phonon Hall effect is well explained by introducing concepts such as time-reversal (\mathcal{T}) symmetry broken, Berry curvature, and Chern number into the phonon systems [7,43]. On the other hand, up to

now, when constructing the phonon Hamiltonian of the open-boundary systems for the natural crystalline materials, quite a lot of works are still following the methods of electronic systems. However, owing to the symmetry requirements of phonon Hamiltonians such as ASR, the reasonability of this processing method should be reassessed.

In the present work, we have discussed the difference in constructing the Wannier tight-binding Hamiltonian between phononic and electronic systems. For simplicity, a 1D monatomic lattice model is presented to illustrate the core idea of this work. Our result shows that the on-site terms of the phonon Hamiltonian of open-boundary systems need the correction of ASR. Furthermore, we reassess the topological phonon states in graphene based on the proposed method. The topologically nontrivial edge states of acoustic phonons are found in free-standing graphene nanoribbons. In addition, the optical modes satisfying ASR are also quite different from those reported previously. When the inversion-time-reversal (\mathcal{PT}) symmetry is broken, along with the splitting of the phonon bands, the distributions of some states will mutate from two edges of the nanoribbon to one edge. Moreover, the topologically nontrivial edge states with nonzero Chern numbers protected by \mathcal{T} symmetry have also been found.

Hamiltonian of 1D monatomic lattice. To start, we consider a 1D monatomic lattice model as shown in Fig. 1, where the blue spheres represent concentrated masses m connected by linear springs with stiffness k . Its dynamical behavior can be investigated by considering the equation of motion for the n th mass

$$m\ddot{u}_n = -k(2u_n - u_{n-1} - u_{n+1}), \quad (1)$$

where u_n represents the displacement of the n th mass away from its equilibrium position. The solution of u_n is sought in the form of Bloch harmonic plane wave

$$u_n(t) = \hat{u}_n e^{-i\omega t} = \tilde{u}_n e^{i(nqa - \omega t)}, \quad (2)$$

where ω and q are the temporal frequency and wavenumber of harmonic motion, respectively. \hat{u}_n and \tilde{u}_n are complex

^{*}keqiuchen@hnu.edu.cn

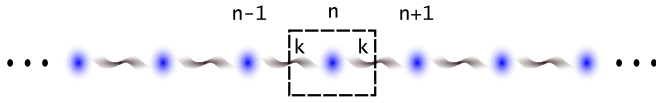


FIG. 1. Schematic of the 1D monatomic lattice.

quantities that define the amplitude of wave motion. According to the recurrence relation between masses described by Eq. (1), the Hamiltonian matrix of this period system can be written as

$$\mathbf{H} = \begin{pmatrix} 2k & -k & 0 & \cdots & 0 & -k \\ -k & 2k & -k & \cdots & 0 & 0 \\ 0 & -k & 2k & \cdots & 0 & 0 \\ \vdots & \vdots & \vdots & \ddots & \vdots & \vdots \\ 0 & 0 & 0 & \cdots & 2k & -k \\ -k & 0 & 0 & \cdots & -k & 2k \end{pmatrix}. \quad (3)$$

The corresponding eigenvalue equation is $\mathbf{H}\mathbf{U} = \lambda\mathbf{U}$, where $\mathbf{U} = (u_1, \dots, u_N)^T$ is the eigenvector, and $\lambda = m\omega^2$ is the eigenvalue. Note that, for the infinite periodic system without external field, the Hamiltonian always satisfies the so-called ASR, i.e., $\sum_{i(j)} \mathbf{H}_{ij} = 0$. In other words, for each row (column) of \mathbf{H} , the value of the on-site term is always equal to the opposite value of the sum of all hopping terms:

$$\mathbf{H}_{ii} = - \sum_{i(j), i \neq j} \mathbf{H}_{ij}. \quad (4)$$

Based on this, when we consider the open-boundary case corresponding to this system, the interaction between the head and tail masses should be removed from the above Hamiltonian. Therefore, the Hamiltonian matrix at open boundary condition can be written as

$$\mathbf{H} = \begin{pmatrix} k & -k & 0 & \cdots & 0 & 0 \\ -k & 2k & -k & \cdots & 0 & 0 \\ 0 & -k & 2k & \cdots & 0 & 0 \\ \vdots & \vdots & \vdots & \ddots & \vdots & \vdots \\ 0 & 0 & 0 & \cdots & 2k & -k \\ 0 & 0 & 0 & \cdots & -k & k \end{pmatrix}. \quad (5)$$

Because of the limitations of Eq. (4), when we remove the hopping terms between the head and tail masses, we also need to rewrite the $2k$ of the on-site terms to k . But for the electronic systems, this step is not required for the on-site terms. Therefore, the Hamiltonian matrix elements of the electronic system is still periodic in the direction away from the boundary, while the phonon system is not. In this toy model, for simplicity, we only consider the nearest neighbor interaction so that just two terms in \mathbf{H} need to be modified, as shown in Eq. (5). Nonetheless, the ASR has a distinct effect on the overall phonon energy level, especially for the addition of acoustic modes (see Supplemental Material [44]). Moreover, the impact of the ASR on the dispersion of phonons will get larger as the number of interacting neighbors increases. The force constant obtained by the first principle calculation based on density functional theory (DFT) is long-range correlation and symmetry broken [45]. Therefore, it is necessary to take the modification of the on-site terms into account when employing the phononic tight-binding (TB) model from the DFT data.

Next, we further discuss the impact of ASR on phonon topological effects through a first-principles calculation example. Previous reports on topological phonons are basically about optical modes in phonon band structure. Recently, the acoustic triple point (ATP) protected by the Nambu-Goldstone theorem was reported to be able to carry a topological charge q if the Euler number of the transverse modes is nonzero [46]. Besides, the corresponding surface-localized states will be found if the phonon group velocity satisfies the condition $v_T/v_L < 1$. Based on this, it has also been reported recently that the ATP of graphene on a TaC(111) substrate is topological, and it will possess a nontrivial nodal charge (the frame-rotation charge) [47]. Topological phonons of free-standing graphene and its corresponding edge states have also been reported previously [14,23]. But interestingly, the edge states of topological acoustic phonons in graphene have never been found before. Therefore, the ASR is expected to have some key impact on the phonon topological effects of graphene.

Computational details. Our calculations are based on the density functional theory (DFT) [48,49] and density functional perturbation theory (DFPT) [50] using the Vienna *ab initio* simulation package (VASP) [51,52]. The interactions of electron-electron and electron-ion are described by the projector augmented-wave (PAW) method [53,54] and Perdew-Burke-Ernzerhof (PBE) functional [55], respectively. The plane-wave cutoff energy is set to 520 eV and the Monkhorst-Pack [56] k-point mesh is used with a size of $13 \times 13 \times 1$ for the Brillouin zone (BZ) sampling. A vacuum layer of 20 Å is used for the unitcell and the $7 \times 7 \times 1$ supercell. In order to get stable crystal structure and reliable force constants, we set the convergence criteria to 10^{-6} eV and 0.001 eV/Å for electronic self-consistency iteration and ionic relaxation, respectively. The PHONONPY code [57] is used to obtain the force constants, which are further used as parameters for building phonon TB Hamiltonians to analyze the topological nature.

The Schrödinger-like equation of phonons, i.e., $\mathbf{H}\psi = \omega\psi$, is adopted to investigate the phonon dispersions [16]. The Hamiltonian matrix has the following form:

$$\mathbf{H} = \begin{pmatrix} 0 & i\mathbf{D}^{1/2} \\ -i\mathbf{D}^{1/2} & -2i\eta \end{pmatrix}, \quad (6)$$

where \mathbf{D} is the dynamical matrix and η is the \mathcal{T} -broken term. The \mathcal{P} symmetry is broken by replacing one of the ^{12}C atoms in the graphene primitive cell with isotope ^{14}C [58], while the \mathcal{T} symmetry is broken by introducing the Raman spin-lattice interaction [7,16,59]. Reference [16] shows the matrix element of the \mathcal{T} -broken term

$$\hat{\eta}_{\mu\nu} = \delta_{\mu\nu} \begin{pmatrix} 0 & -\Omega_z & \Omega_y \\ \Omega_z & 0 & -\Omega_x \\ -\Omega_y & \Omega_x & 0 \end{pmatrix}, \quad (7)$$

where $\delta_{\mu\nu}$ is the Kronecker delta function. We set the parameters $\Omega_z = 0.1$ and $\Omega_x = \Omega_y = 0$ so that the direction of the external field is set to be perpendicular to the graphene plane. To display the localization features of topological surface states, the nonequilibrium Green's function (NEGF) method, which has been widely used for many-body quantum transport [60–65], is adopted to calculate the surface local density of

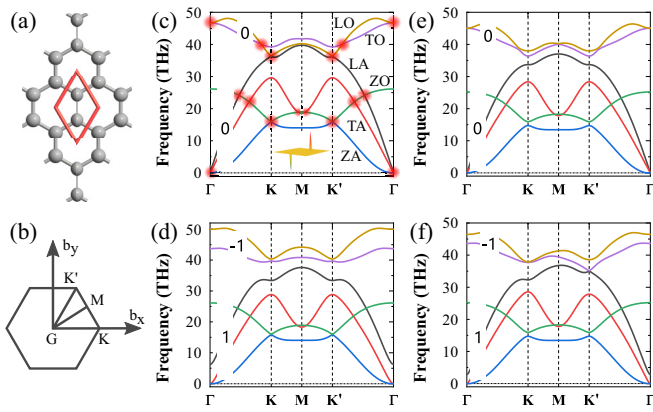


FIG. 2. Phonon dispersions of graphene under various circumstances. (a) Honeycomb lattice of graphene, where the primitive cell shows inside the red line. (b) The high-symmetry path in BZ for phonon band structure calculation. (c) Phonon dispersions of graphene with \mathcal{PT} symmetry, where the DPs are marked with red dots. The inset is the distribution of Berry curvature in the BZ corresponding to the 1–4 bands. Phonon dispersions with the Chern numbers labeled on the bulk bands of graphene with \mathcal{T} -broken, \mathcal{P} -broken and \mathcal{PT} -broken are shown in (d), (e), and (f), respectively. Here, the \mathcal{P} symmetry is broken by replacing one of the C atoms in graphene primitive cell with isotope ^{14}C , while the \mathcal{T} symmetry is broken by introducing the Raman spin-lattice interaction.

states (LDOS). However, the Hamiltonian described by the Schrödinger-like equation of phonons contains the $\mathbf{D}^{1/2}$ term, which makes it impossible to handle the left and right semi-infinite leads independently. Here, we calculate the surface LDOS by using the generalized NEGF method [16,66].

Phonon dispersion of graphene. We first calculate the phonon band structure of free-standing graphene. The primitive cell of graphene and the high-symmetry path in BZ for phonon band structure calculations are shown in Figs. 2(a) and 2(b), respectively. Phonon dispersions in each case are presented in Figs. 2(c)–2(f). It is seen that, when the system has \mathcal{PT} symmetry, there are several degenerate points (DPs) in the phonon spectrum marked by red points in Fig. 2(c), including the ATP, which is consistent with previous reports [23,45]. While some of the DPs will open a band gap when any of the \mathcal{PT} symmetry is broken, as shown in Figs. 2(d)–2(f) specifically. At K and K', the DPs formed by longitudinal acoustic (LA) and longitudinal optical (LO) bands at about 36 THz will always open a full band gap when \mathcal{P}/\mathcal{T} symmetry is broken. The results with symmetry broken above are consistent with previous reports about the 2D honeycomb lattice model [16].

Therefore, we further calculate the Chern number of the 1–4 and 5–6 bands under various circumstances, and the results are labeled on the bands. Importantly, the fact that the band gap between LA and LO branches is topologically nontrivial is confirmed by the nonzero Chern numbers when the \mathcal{T} symmetry is broken. This is also consistent with the results of previously reported models [8,16]. Hence, gapless one-way edge states are expected to emerge in this topologically nontrivial band gap.

It should be noted that the nodal charge of the ATP is -1 [47], although the Chern number is zero when the system has

\mathcal{T} symmetry. Moreover, the group velocities of the acoustic phonons in Fig. 2(c) satisfy the condition $v_T/v_L < 1$. These results mean that the ATP of graphene is topologically nontrivial with \mathcal{PT} symmetry, and meanwhile the topological ATP will also correspond to topologically nontrivial edge states [46].

Edge states of the zigzag graphene nanoribbons. To verify the existence of such edge states, we construct a phonon TB model for the zigzag graphene nanoribbon (ZGNR) with a thickness of 20 layers [Fig. 3(a)]. The ZGNR has a vacuum layer of 20 Å in the aperiodic directions. The phonon dispersions of the ZGNR with no \mathcal{PT} -broken are shown in Figs. 3(b) and 3(c). When no ASR is performed, there are no acoustic modes in the phonon spectrum of ZGNR, as shown in Fig. 3(b), which leads to unphysical results. However, the whole phonon spectrum will be reasonable when the ASR is performed for the Hamiltonian of ZGNR. Concretely, after the correction of ASR, the acoustic modes appear, as shown by the thick green lines in Fig. 3(c). Moreover, two of these acoustic modes, which are labeled as M_2 in Fig. 3(c), appear in the local band gap of 14–18 THz around the X point. Besides, the group velocities of the modes marked by yellow lines, which are labeled as M_1 in Fig. 3(c), have changed dramatically. Meanwhile, the modes at about 30 THz around X point [as shown in Fig. 3(b) with red dashed frame] disappear. These significant changes argue the importance of performing the correction of ASR in constructing the phonon TB Hamiltonian based on first-principles calculations.

Next, based on the TB Hamiltonian with ASR correction, we introduce the \mathcal{P} -broken term and \mathcal{T} -broken term to the ZGNR phonon system in succession, and the phonon dispersions are shown in Fig. 3(d) and 3(e), respectively. On the one hand, the twofold degeneracy of M_1 and M_2 are both eliminated when the \mathcal{P} symmetry is broken [Fig. 3(d)]. The twofold degeneracy of M_1 will not be eliminated when only the \mathcal{T} -broken term is introduced into this system [Fig. 3(e)]. This means that the distributions of these edge states corresponding to M_1 and M_2 will be changed if their degeneracy is eliminated after \mathcal{PT} -broken. On the other hand, at about 38 THz, a pair of phonon modes with a linear crossing point labeled as M_3 in Fig. 3(e) appear in the full band gap, which corresponds to the nonzero Chern number of the bulk band [Fig. 2(d)]. Meanwhile, the armchair edges of graphene ribbons can also possess phonon edge states in the full band gap at about 38 THz (The details are shown in the Supplemental Material [44]). Since no bulk modes exist in the full gap, M_3 cannot scatter into the bulk of the ZGNR. Besides, based on the TB Hamiltonian without ASR correction, the phonon dispersions with \mathcal{P} -broken and \mathcal{T} -broken have also been calculated, and the results generally have a large deviation from the case with ASR, as shown in the Supplemental Material [44].

To make this more clear, as shown in Fig. 4(e), we draw the state distributions of some representative points labeled in Figs. 4(a)–4(d), which are the zoom-in local phonon dispersions corresponding to the areas with purple dashed frame in Figs. 3(c)–3(e). M_1 will keep twofold degeneracy when the system have \mathcal{P} symmetry, and M_2 will keep twofold degeneracy when the system have \mathcal{PT} symmetry. Therefore, Pa_1/Pa_2 , $\text{Pa}'_1/\text{Pa}'_2$, and Pb_1/Pb_2 possess states that are localized on the upper and lower edges of ZGNR simultaneously. When

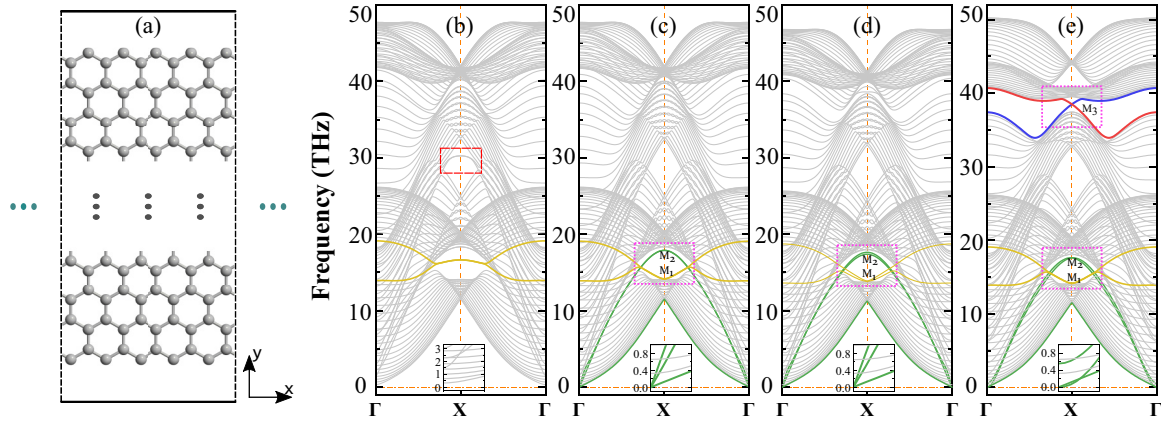


FIG. 3. Phonon dispersions of ZGNR under various circumstances. (a) Schematic of the ZGNR. The x direction has periodicity and the y direction has a vacuum layer of 20 \AA . (b), (c) Phonon dispersions of ZGNR with \mathcal{TP} symmetry with and without the correction of ASR, respectively. The acoustic modes appear after the correction. (d), (e) Phonon spectrum of ZGNR with \mathcal{P} -broken and \mathcal{T} -broken based on the correction of ASR, respectively. There are three pairs of phonon modes labeled as M_1 , M_2 and M_3 in the band gaps at about 16 THz and 38 THz around X. The insets in (b)–(e) are the zoom-in local phonon dispersions around Γ .

the degeneracy is eliminated, the distributions of these edge states corresponding to $\text{Pa}'_1/\text{Pa}'_2$, $\text{Pb}'_1/\text{Pb}'_2$, and $\text{Pb}''_1/\text{Pb}''_2$ are only localized on one edge of ZGNR. Further, the local states of Pc_1/Pc_2 represent the standard Chern insulator topological nontrivial edge states.

We further compute the LDOS and phonon transmission spectra of ZGNR by iterating the surface Green's functions with \mathcal{T} -broken. Figures 5(a)–5(c) show the projected LDOS of the down edge, bulk, and up edge of ZGNR, respectively. Obviously, M_2 is split into two different phonon modes, which are localized on the lower and upper boundaries of ZGNR respectively, and so does the M_3 . On the other hand, M_1 maintains a twofold degeneracy, while being localized on the two boundaries. The effects of disorder on transmission spectrum are shown in Fig. 5(d). Here, we regulate the disorder by doping different carbon isotopes with the concentration of 10%

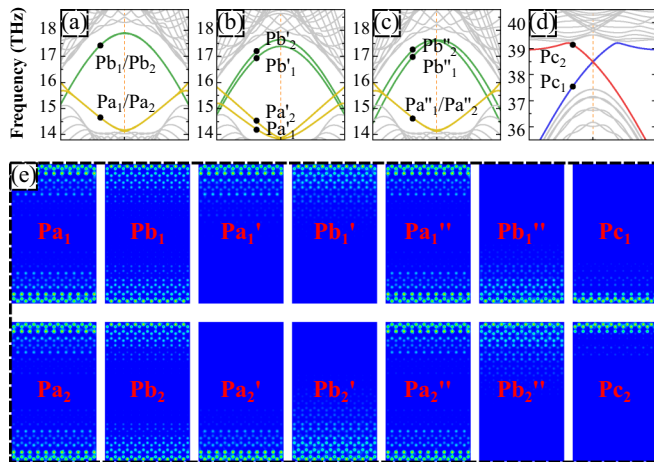


FIG. 4. Local states distribution of ZGNR in real space. (a)–(d) phonon dispersions corresponding to the areas with purple dashed frame in Figs. 3(c)–3(e). Some points with $q_x = 0.45$ are marked on the phonon band structure. (e) The local states of ZGNR corresponding to the points marked in (a)–(d).

randomly. We can find that the total probability of phonon transmission decreases as the mass of the isotope increases, except for the one-way edge states within the bulk gap at about 38 THz. This is exactly the standard feature of surface states that are immune to backscattering in Chern insulators.

Discussions and perspectives. Our results show that, in order to get a phonon spectrum with reasonable acoustic branches when dealing with open boundary phonon systems, we should modify the on-site terms of the TB Hamiltonian according to the ASR. In practice, we usually obtain the on-site terms according to Eq. (4) to satisfy the ASR naturally rather than correction. The ASR makes the part of Hamiltonian corresponding to the surface atoms no longer periodic. Thus, the surface part should be treated as scattering regions when solving the Green's functions. Furthermore, graphene, with space group $P6/mmm$ (No. 191), is a typical two-dimensional honeycomb lattice material and an ideal platform for realizing various novel physical effects [67,68]. The topological

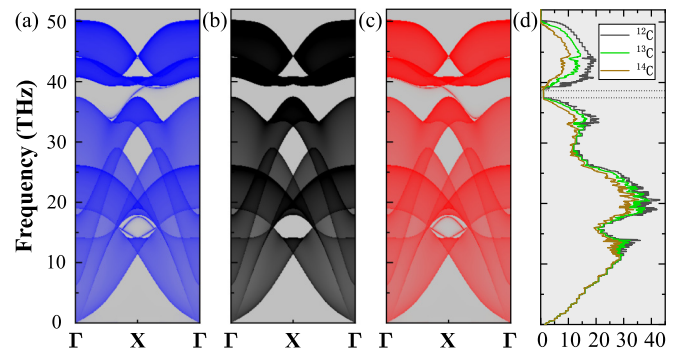


FIG. 5. Local density of states and transmission spectrum with the \mathcal{T} symmetry broken. (a)–(c) Density of states projected onto the down edge, bulk and up edge of ZGNR, respectively. (d) Phonon transmission under different carbon isotope doping, where the doping concentration is always 10%. The probability of phonon transmission decreases as the mass of the isotope increases, except for the one-way edge states within the bulk gap.

properties of electrons and phonons in graphene tend to be robust to environmental changes, so that carbon allotropes constructed from graphene can often exhibit excellent properties in various aspects. Therefore, the tuning of the topological properties of surface states by various means, such as gating [69,70] and twisting [71,72], also needs further investigation.

Conclusion. In conclusion, we show the necessity of ASR for the construction of the phonon TB Hamiltonian. Furthermore, we find topological phonons in both acoustic and optical branches of graphene, and the corresponding topologically nontrivial edge phonon modes are also observed. It is worth mentioning that the diverse topological phonon states in graphene respond differently to the \mathcal{PT} symmetry of the

system. Interestingly, the distributions of some edge states can mutate from two edges of the nanoribbon to one edge at the same time as the band splitting when the \mathcal{PT} symmetry is broken. These results indicate that graphene is indeed an ideal platform for realizing phonon topological effects, and it is very possible to realize novel physical effects such as phonon-based information conduction, quantum interference, thermal superconductivity, and other phononic devices based on this in the future.

Acknowledgments. This work was supported by the National Natural Science Foundation of China (Grant No. 11974106). Numerical computations were performed at the National Supercomputer Center in Changsha.

-
- [1] N. Li, J. Ren, L. Wang, G. Zhang, P. Hänggi, and B. Li, Colloquium: Phononics: Manipulating heat flow with electronic analogs and beyond, *Rev. Mod. Phys.* **84**, 1045 (2012).
- [2] S. D. Huber, Topological mechanics, *Nat. Phys.* **12**, 621 (2016).
- [3] R. Süsstrunk and S. D. Huber, Classification of topological phonons in linear mechanical metamaterials, *Proc. Natl. Acad. Sci.* **113**, E4767 (2016).
- [4] Y. Liu, Y. Xu, and W. Duan, Berry phase and topological effects of phonons, *Natl. Sci. Rev.* **5**, 314 (2018).
- [5] G. Ma, M. Xiao, and C. T. Chan, Topological phases in acoustic and mechanical systems, *Nat. Rev. Phys.* **1**, 281 (2019).
- [6] Y. Liu, X. Chen, and Y. Xu, Topological phononics: From fundamental models to real materials, *Adv. Funct. Mater.* **30**, 1904784 (2020).
- [7] L. Zhang, J. Ren, J.-S. Wang, and B. Li, Topological Nature of the Phonon Hall Effect, *Phys. Rev. Lett.* **105**, 225901 (2010).
- [8] P. Wang, L. Lu, and K. Bertoldi, Topological Phononic Crystals with One-Way Elastic Edge Waves, *Phys. Rev. Lett.* **115**, 104302 (2015).
- [9] Y.-T. Wang, P.-G. Luan, and S. Zhang, Coriolis force induced topological order for classical mechanical vibrations, *New J. Phys.* **17**, 073031 (2015).
- [10] V. Peano, C. Brendel, M. Schmidt, and F. Marquardt, Topological Phases of Sound and Light, *Phys. Rev. X* **5**, 031011 (2015).
- [11] Z. Yang, F. Gao, X. Shi, X. Lin, Z. Gao, Y. Chong, and B. Zhang, Topological Acoustics, *Phys. Rev. Lett.* **114**, 114301 (2015).
- [12] A. B. Khanikaev, R. Fleury, S. H. Mousavi, and A. Alu, Topologically robust sound propagation in an angular-momentum-biased graphene-like resonator lattice, *Nat. Commun.* **6**, 8260 (2015).
- [13] R. Fleury, A. B. Khanikaev, and A. Alu, Floquet topological insulators for sound, *Nat. Commun.* **7**, 11744 (2016).
- [14] T. Kariyado and Y. Hatsugai, Manipulation of Dirac cones in mechanical graphene, *Sci. Rep.* **5**, 18107 (2016).
- [15] M. Xiao, W.-J. Chen, W.-Y. He, and C. T. Chan, Synthetic gauge flux and Weyl points in acoustic systems, *Nat. Phys.* **11**, 920 (2015).
- [16] Y. Liu, Y. Xu, S.-C. Zhang, and W. Duan, Model for topological phononics and phonon diode, *Phys. Rev. B* **96**, 064106 (2017).
- [17] Y. Liu, C.-S. Lian, Y. Li, Y. Xu, and W. Duan, Pseudospins and Topological Effects of Phonons in a Kekulé Lattice, *Phys. Rev. Lett.* **119**, 255901 (2017).
- [18] Y. Liu, Y. Xu, and W. Duan, Three-dimensional topological states of phonons with tunable pseudospin physics, *Research* **2019**, 5173580 (2019).
- [19] L. M. Nash, D. Kleckner, A. Read, V. Vitelli, A. M. Turner, and W. T. Irvine, Topological mechanics of gyroscopic metamaterials, *Proc. Natl. Acad. Sci.* **112**, 14495 (2015).
- [20] Y. Yang, H.-x. Sun, J.-p. Xia, H. Xue, Z. Gao, Y. Ge, D. Jia, S.-q. Yuan, Y. Chong, and B. Zhang, Topological triply degenerate point with double Fermi arcs, *Nat. Phys.* **15**, 645 (2019).
- [21] B. Xie, H. Liu, H. Cheng, Z. Liu, S. Chen, and J. Tian, Experimental Realization of Type-II Weyl Points and Fermi Arcs in Phononic Crystal, *Phys. Rev. Lett.* **122**, 104302 (2019).
- [22] Y. Jin, R. Wang, and H. Xu, Recipe for Dirac phonon states with a quantized valley Berry phase in two-dimensional hexagonal lattices, *Nano Lett.* **18**, 7755 (2018).
- [23] J. Li, L. Wang, J. Liu, R. Li, Z. Zhang, and X.-Q. Chen, Topological phonons in graphene, *Phys. Rev. B* **101**, 081403(R) (2020).
- [24] Z. J. Chen, R. Wang, B. W. Xia, B. B. Zheng, Y. J. Jin, Y.-J. Zhao, and H. Xu, Three-Dimensional Dirac Phonons with Inversion Symmetry, *Phys. Rev. Lett.* **126**, 185301 (2021).
- [25] T. Zhang, Z. Song, A. Alexandradinata, H. Weng, C. Fang, L. Lu, and Z. Fang, Double-Weyl Phonons in Transition-Metal Monosilicides, *Phys. Rev. Lett.* **120**, 016401 (2018).
- [26] H. Miao, T. T. Zhang, L. Wang, D. Meyers, A. H. Said, Y. L. Wang, Y. G. Shi, H. M. Weng, Z. Fang, and M. P. M. Dean, Observation of Double Weyl Phonons in Parity-Breaking FeSi, *Phys. Rev. Lett.* **121**, 035302 (2018).
- [27] J. Liu, W. Hou, E. Wang, S. Zhang, J.-T. Sun, and S. Meng, Ideal type-II Weyl phonons in wurtzite CuI, *Phys. Rev. B* **100**, 081204(R) (2019).
- [28] B. W. Xia, R. Wang, Z. J. Chen, Y. J. Zhao, and H. Xu, Symmetry-Protected Ideal Type-II Weyl Phonons in CdTe, *Phys. Rev. Lett.* **123**, 065501 (2019).
- [29] T. Zhang, L. Lu, S. Murakami, Z. Fang, H. Weng, and C. Fang, Diagnosis scheme for topological degeneracies crossing high-symmetry lines, *Phys. Rev. Research* **2**, 022066 (2020).
- [30] J. Li, J. Liu, S. A. Baronett, M. Liu, L. Wang, R. Li, Y. Chen, D. Li, Q. Zhu, and X.-Q. Chen, Computation and data driven discovery of topological phononic materials, *Nat. Commun.* **12**, 1204 (2021).

- [31] J. Li, Q. Xie, J. Liu, R. Li, M. Liu, L. Wang, D. Li, Y. Li, and X.-Q. Chen, Phononic weyl nodal straight lines in mgb 2, *Phys. Rev. B* **101**, 024301 (2020).
- [32] Y. Liu, N. Zou, S. Zhao, X. Chen, Y. Xu, and W. Duan, Ubiquitous topological states of phonons in solids: Silicon as a model material, *Nano Lett.* **22**, 2120 (2022).
- [33] B. Zheng, B. Xia, R. Wang, Z. Chen, J. Zhao, Y. Zhao, and H. Xu, Ideal type-iii nodal-ring phonons, *Phys. Rev. B* **101**, 100303 (2020).
- [34] Y. J. Jin, Z. J. Chen, B. W. Xia, Y. J. Zhao, R. Wang, and H. Xu, Ideal intersecting nodal-ring phonons in bcc c 8, *Phys. Rev. B* **98**, 220103 (2018).
- [35] Z. Wang, W. Zhou, A. N. Rudenko, and S. Yuan, Lattice dynamics and topological surface phonon states in cuprous oxide cu 2 o, *Phys. Rev. B* **103**, 195137 (2021).
- [36] B. Li, L. Wang, and G. Casati, Thermal Diode: Rectification of Heat Flux, *Phys. Rev. Lett.* **93**, 184301 (2004).
- [37] B. Li, L. Wang, and G. Casati, Negative differential thermal resistance and thermal transistor, *Appl. Phys. Lett.* **88**, 143501 (2006).
- [38] C. Fan, Y. Gao, and J. Huang, Shaped graded materials with an apparent negative thermal conductivity, *Appl. Phys. Lett.* **92**, 251907 (2008).
- [39] G. Xu, Y. Yang, X. Zhou, H. Chen, A. Alù, and C.-W. Qiu, Diffusive topological transport in spatiotemporal thermal lattices, *Nat. Phys.* **18**, 450 (2022).
- [40] G. Xu, W. Li, X. Zhou, H. Li, Y. Li, S. Fan, S. Zhang, D. N. Christodoulides, and C.-W. Qiu, Observation of weyl exceptional rings in thermal diffusion, *Proc. Natl. Acad. Sci.* **119**, e2110018119 (2022).
- [41] D. M. Rowe, *Thermoelectrics Handbook: Macro to Nano* (CRC Press, 2018).
- [42] X.-H. Cao, D. Wu, J. Zeng, N.-N. Luo, W.-X. Zhou, L.-M. Tang, and K.-Q. Chen, Controllable anisotropic thermoelectric properties in 2d covalent organic radical frameworks, *Appl. Phys. Lett.* **119**, 263901 (2021).
- [43] C. Strohm, G. L. J. A. Rikken, and P. Wyder, Phenomenological Evidence for the Phonon Hall Effect, *Phys. Rev. Lett.* **95**, 155901 (2005).
- [44] See Supplemental Material at <http://link.aps.org/supplemental/10.1103/PhysRevB.106.L121401> for more details about the phonon bands of 1D monatomic lattice, band structure of ZGNR done without ASR when \mathcal{P} -broken or \mathcal{T} -broken and band structure of GNR with armchair boundary.
- [45] N. Mounet and N. Marzari, First-principles determination of the structural, vibrational and thermodynamic properties of diamond, graphite, and derivatives, *Phys. Rev. B* **71**, 205214 (2005).
- [46] S. Park, Y. Hwang, H. C. Choi, and B.-J. Yang, Topological acoustic triple point, *Nat. Commun.* **12**, 6781 (2021).
- [47] G. F. Lange, A. Bouhon, B. Monserrat, and R.-J. Slager, Topological continuum charges of acoustic phonons in two dimensions and the nambu-goldstone theorem, *Phys. Rev. B* **105**, 064301 (2022).
- [48] P. Hohenberg and W. Kohn, Inhomogeneous electron gas, *Phys. Rev.* **136**, B864 (1964).
- [49] W. Kohn and L. J. Sham, Self-consistent equations including exchange and correlation effects, *Phys. Rev.* **140**, A1133 (1965).
- [50] S. Baroni, S. De Gironcoli, A. Dal Corso, and P. Giannozzi, Phonons and related crystal properties from density-functional perturbation theory, *Rev. Mod. Phys.* **73**, 515 (2001).
- [51] G. Kresse and J. Furthmüller, Efficiency of ab-initio total energy calculations for metals and semiconductors using a plane-wave basis set, *Comput. Mater. Sci.* **6**, 15 (1996).
- [52] G. Kresse and J. Furthmüller, Efficient iterative schemes for ab initio total-energy calculations using a plane-wave basis set, *Phys. Rev. B* **54**, 11169 (1996).
- [53] P. E. Blöchl, Projector augmented-wave method, *Phys. Rev. B* **50**, 17953 (1994).
- [54] G. Kresse and D. Joubert, From ultrasoft pseudopotentials to the projector augmented-wave method, *Phys. Rev. B* **59**, 1758 (1999).
- [55] J. P. Perdew, K. Burke, and M. Ernzerhof, Generalized Gradient Approximation Made Simple, *Phys. Rev. Lett.* **77**, 3865 (1996).
- [56] H. J. Monkhorst and J. D. Pack, Special points for brillouin-zone integrations, *Phys. Rev. B* **13**, 5188 (1976).
- [57] A. Togo and I. Tanaka, First principles phonon calculations in materials science, *Scr. Mater.* **108**, 1 (2015).
- [58] L. Zhang and Q. Niu, Chiral Phonons at High-Symmetry Points in Monolayer Hexagonal Lattices, *Phys. Rev. Lett.* **115**, 115502 (2015).
- [59] L. Sheng, D. N. Sheng, and C. S. Ting, Theory of the Phonon Hall Effect in Paramagnetic Dielectrics, *Phys. Rev. Lett.* **96**, 155901 (2006).
- [60] J.-S. Wang, J. Wang, and J. Lü, Quantum thermal transport in nanostructures, *Eur. Phys. J. B* **62**, 381 (2008).
- [61] Y. Xu, X. Chen, J.-S. Wang, B.-L. Gu, and W. Duan, Thermal transport in graphene junctions and quantum dots, *Phys. Rev. B* **81**, 195425 (2010).
- [62] J.-S. Wang, B. K. Agarwalla, H. Li, and J. Thingna, Nonequilibrium green's function method for quantum thermal transport, *Front. Phys.* **9**, 673 (2014).
- [63] M. Paulsson, T. Frederiksen, and M. Brandbyge, Modeling inelastic phonon scattering in atomic-and molecular-wire junctions, *Phys. Rev. B* **72**, 201101 (2005).
- [64] Y. Xu, J.-S. Wang, W. Duan, B.-L. Gu, and B. Li, Nonequilibrium green's function method for phonon-phonon interactions and ballistic-diffusive thermal transport, *Phys. Rev. B* **78**, 224303 (2008).
- [65] H. Pan, L.-M. Tang, and K.-Q. Chen, Quantum mechanical modeling of magnon-phonon scattering heat transport across three-dimensional ferromagnetic/nonmagnetic interfaces, *Phys. Rev. B* **105**, 064401 (2022).
- [66] Y.-J. Zeng, Z.-K. Ding, H. Pan, Y.-X. Feng, and K.-Q. Chen, Nonequilibrium green's function method for phonon heat transport in quantum system, *J. Phys.: Condens. Matter* **34**, 223001 (2022).
- [67] A. K. Geim, Graphene: Status and prospects, *Science* **324**, 1530 (2009).
- [68] A. K. Geim and K. S. Novoselov, The rise of graphene, in *Nanoscience and Technology: A Collection of Reviews from Nature Journals* (World Scientific, 2010), pp. 11–19.
- [69] Q. Liu, J.-J. Li, D. Wu, X.-Q. Deng, Z.-H. Zhang, Z.-Q. Fan, and K.-Q. Chen, Gate-controlled reversible rectifying behavior investigated in a two-dimensional mos 2 diode, *Phys. Rev. B* **104**, 045412 (2021).

- [70] D. Wu, X.-H. Cao, P.-Z. Jia, Y.-J. Zeng, Y.-X. Feng, L.-M. Tang, W.-X. Zhou, and K.-Q. Chen, Excellent thermoelectric performance in weak-coupling molecular junctions with electrode doping and electrochemical gating, *Sci. China Phys. Mech. Astron.* **63**, 276811 (2020).
- [71] D. Wu, L. Huang, P.-Z. Jia, X.-H. Cao, Z.-Q. Fan, W.-X. Zhou, and K.-Q. Chen, Tunable spin electronic and thermoelectric properties in twisted triangulene π -dimer junctions, *Appl. Phys. Lett.* **119**, 063503 (2021).
- [72] Y.-J. Zeng, Y.-X. Feng, L.-M. Tang, and K.-Q. Chen, Effect of out-of-plane strain on the phonon structures and anharmonicity of twisted multilayer graphene, *Appl. Phys. Lett.* **118**, 183103 (2021).